In vivo detection of amyloid plaques in a mouse model of Alzheimer's disease

Daniel M. Skovronsky*, Bin Zhang*, Mei-Ping Kung†, Hank F. Kung†‡, John Q. Trojanowski*, and Virginia M.-Y. Lee*§

Center for Neurodegenerative Disease Research, Departments of *Pathology and Laboratory Medicine, †Radiology, and ‡Pharmacology, University of Pennsylvania School of Medicine, Philadelphia, PA 19104

Edited by Britton Chance, University of Pennsylvania, Philadelphia, PA, and approved April 27, 2000 (received for review March 2, 2000)

Strategies for treating Alzheimer's disease (AD) include therapies designed to decrease senile plaque (SP) formation and/or promote clearance of SPs, but clinical trials of these treatments are limited by the lack of effective methods to monitor changes in plaque burden in the brains of living AD patients. However, because SPs are extracellular deposits of amyloid-β peptides (Aβ), it may be possible to eventually develop radioligands that cross the blood–brain barrier (BBB) and label SPs so they can be visualized by current imaging methods. As a first step toward the generation of such a radioligand, we developed a probe, [(*trans,trans*)-1-bromo-2,5-bis-(3-hydroxycarbonyl-4-hydroxy)styrylbenzene (BSB)], and we report here that BSB has the following properties essential for a probe that can detect SPs *in vivo*. First, BSB sensitively labels SPs in AD brain sections. Second, BSB permeates living cells in culture and binds specifically to intracellular Aβ aggregates. Third, after intracerebral injection in living transgenic mouse models of AD amyloidosis, BSB labels SPs composed of human Aβ with high sensitivity and specificity. Fourth, BSB crosses the BBB and labels numerous AD-like SPs throughout the brain of the transgenic mice after i.v. injection. Thus, we conclude that BSB is an appropriate starting point for future efforts to generate an antemortem diagnostic for AD.

amyloid β-protein | imaging | senile plaques

The amyloid cascade hypothesis proposes that the onset and progression of Alzheimer's disease (AD) results from increased production of amyloid-β peptides (Aβ) and the progressive accumulation of Aβ in senile plaques (SPs) (reviewed in ref. 1). Further, because SPs initiate inflammatory responses that are neurotoxic, the long-term consequences of Aβ amyloidosis are progressive neuronal loss and dementia. Support for this hypothesis stems from observations that mutations pathogenic for familial AD (FAD) increase the production of the more amyloidogenic 42-aa-long Aβ peptide ($A\beta_{1-42}$) (2–6). Moreover, overexpression of FAD mutants in transgenic mice produces increased Aβ followed by Aβ deposition in AD-like SPs (7–9). Nonetheless, SPs have not been directly linked to the onset of dementia, and proof of the amyloid cascade hypothesis remains incomplete. However, the recent development of strategies to decrease the burden of SPs (10, 11) presents novel opportunities to definitively test the amyloid hypothesis in clinical trials of these therapies, but this requires reliable and sensitive methods to monitor plaque burden in the brains of living AD patients.

Although there are many methods to detect SPs by staining postmortem brain tissue, none are available to monitor SPs in living patients. However, a blood–brain barrier (BBB) permeable radio probe specific for SPs should enable single-positron emission computed tomography or positron emission tomography visualization of these lesions in AD patients. Significantly, the availability of probes to image SPs would facilitate *in vivo* diagnosis of AD and the evaluation of therapies meant to decrease plaque burden in AD. Attempts to develop such probes have focused on Chrysamine G (CG; ref. 12), a derivative of Congo red that also binds Aβ *in vitro* and in postmortem AD brain sections. Unlike Congo red, CG could be a potential probe for detecting SPs *in vivo* because it crosses the BBB of mice (13). Indeed (99 m), technetium (Tc)-labeled CG [(99 m)Tc-MAMA-CG] has been synthesized and labels plaques in postmortem sections of AD brains (14). Moreover, Klunk *et al.* (15) synthesized X-34, a fluorescent CG derivative that labels plaques in postmortem AD brain sections and that also may cross the BBB. No probe has been shown to label SPs *in vivo*, which is required of a ligand used for imaging plaques in AD patients.

Here we report the biological properties of a probe for SPs [(*trans,trans*),-1-bromo-2,5-bis-(3-hydroxycarbonyl-4-hydroxy)styrylbenzene (BSB)]. To develop this probe, we devised a simple synthetic method to produce BSB and demonstrated that it has a high binding affinity for Aβ aggregates *in vitro* (K_i = 0.4 μM) (Z. P. Zhuang and H.F.K., personal communication). Like X-34 and CG, BSB specifically labels SPs in postmortem AD brain sections (Zhuang and H.F.K., personal communication). For these reasons, and because of the excellent fluorescent properties (λ_{ab} = 340 nm; λ_{em} = 520 nm) and lipophilicity of BSB, we evaluated the usefulness of this Aβ-specific ligand for *in vivo* investigations of amyloid deposition. Here, we use two complementary *in vivo* model systems to show that BSB effectively labels Aβ aggregates *in vivo*.

Materials and Methods

Neuropathological Staining. Brains of AD (n = 3) and normal control patients (n = 3) were obtained at autopsy, and neuropathological diagnosis was confirmed by current criteria (16). To do this, we performed a variety of studies using 6-μm-thick serial sections of paraffin-embedded blocks of hippocampus and cortex from brains fixed in 70% ethanol (EtOH)/150 mM NaCl. For BSB staining, sections were immersed in 0.01% (200 μM) to 0.5% (10 mM) BSB in 50% EtOH for 30 min. Sections were quickly differentiated in saturated Li_2CO_3 and rinsed in 50% EtOH before examination by fluorescent microscopy. For staining with thioflavin-S (TF-S), serial sections of brain tissue were immersed in 10% neutral buffered formalin for 1 h, followed by bleaching of lipofuscin in 0.05% $KMnO_4$ and destaining in 0.2% $K_2S_2O_5$/0.2% oxalic acid before staining with TF-S for 3 min (0.0125% TF-S in 40% EtOH). Sections were quickly differentiated in 50% EtOH before examination by fluorescent microscopy. Immunostaining was accomplished by using the mAb 4G8 (Senetek PLC, St. Louis, MO) or the anti-Aβ polyclonal antiserum 2332. Labeling was detected by using the avidin–biotin

This paper was submitted directly (Track II) to the PNAS office.

Abbreviations: Aβ, amyloid-β peptide; $A\beta_{1-40}$, $A\beta_{1-42}$, 40- and 42-aa-long forms of Aβ, respectively; AD, Alzheimer's disease; BBB, blood–brain barrier; SP, senile plaque; CG, chrysamine G; TF-S, thioflavine-S; BSB, (*trans,trans*)-1-bromo-2,5-bis-(3-hydroxycarbonyl-4-hydroxy)styrylbenzene; NFTs, neurofibrillary tangles.

§To whom reprint requests should be addressed. E-mail: vmylee@mail.med.upenn.edu.

The publication costs of this article were defrayed in part by page charge payment. This article must therefore be hereby marked "*advertisement*" in accordance with 18 U.S.C. §1734 solely to indicate this fact.

peroxidase kit (Vector-stain ABC Kit; Vector Laboratories) and 3,3′-diaminobenzidine tetrahydrochloride.

Fibroblast Aβ Treatment and Staining. Human foreskin fibroblasts (CC92; American Type Culture Collection) were grown in RPMI 1640 with 10% FBS and penicillin/streptomycin to 70–80% confluency in 24-well plates and treated with 1 μg/ml to 50 μg/ml synthetic $A\beta_{1-42}$ (Bachem) or 5 μg/ml synthetic $A\beta_{42-1}$ for 18 h. Fibroblasts were removed by trypsinization and replated on 12-mm cover slips and allowed to recover 24 h. For direct staining, fibroblasts were then fixed in 95% EtOH, 5% acetic acid and stained with BSB or TF-S, as described above. For *in vivo* staining, 0.005% BSB or 0.005% TF-S was added to the tissue culture medium, and Aβ-loaded fibroblasts were allowed to take up the compounds for 2 h. Cells were then washed in PBS, fixed, and examined by fluorescent microscopy.

Quantitation of Intracellular Aβ. Aβ-treated fibroblasts were trypsinized and replated as before. After 24 h, cells were washed twice with PBS and scraped into PBS. Cells were pelleted by centrifugation at 2,000 × *g* for 2 min and were then lysed in 100 μl 70% formic acid. Insoluble material was pelleted by centrifugation at 40,000 × *g* at 4°C for 20 min, and the supernatant was neutralized by adding 1.9 ml × 1 M Tris base and diluted 1:3 in H_2O before quantification of Aβ by sandwich ELISA. Sandwich ELISA was performed as described previously by using the mAbs BAN-50 (specific for the first 10 amino acids of Aβ), horseradish peroxidase-conjugated BA-27 (specific for $A\beta_{1-40}$), and horseradish peroxidase-conjugated BC-05 (specific for $A\beta_{1-42}$) (3, 17).

Injection and *in Vivo* Characterization of BSB. In this study, 11- to 16-mo-old Tg2576 transgenic and age-matched control mice were anesthetized with ketamine/xylazine before mounting in a stereotactic apparatus. For intrahippocampal injections, 3 μl of 0.04% BSB in 2% DMSO or vehicle alone were injected at 2 mm posterior to bregma, 2 mm lateral to the midline, and 2 mm below the skull surface. For intraventricular injections, 9 μl of 0.08% BSB in 4% DMSO was injected at 0.35 mm posterior to bregma, 1.2 mm lateral to the midline, and 2 mm below the skull surface. For i.v. injections, the tail vein of anesthetized Tg2576 and control mice was visualized by dissection, and 500 μl of 0.2% BSB in 10% DMSO was injected in 7 boluses over 6 h. In each case, mice were allowed to recover for 30 min, 3 h, or 18 h before they were killed by decapitation and brains were removed and frozen. Eight- to ten-micrometer sections were cut by cryostat, dried, and imaged with no additional staining. After imaging, selected sections were stained with TF-S or immunostained with mAb 4G8 as described above.

Results

BSB Labels SPs in Sections of Postmortem AD Brain. Because BSB binds aggregated Aβ *in vitro* (Z. P. Zhuang and H.F.K., personal communication), we assessed its ability to bind β-amyloid in SPs. Cortical sections from pathologically confirmed postmortem AD cases were stained with BSB, which is highly fluorescent, thus staining was visualized by fluorescence microscopy. For purposes of comparison, we stained serial sections with thioflavin-S (TF-S), because TF-S is commonly used to stain SPs and neurofibrillary tangles (NFTs) for the postmortem diagnosis of AD. As shown in Fig. 1*A*, BSB labeled SPs in AD cortex with comparable sensitivity and fluorescent intensity as TF-S (Fig. 1*B*). In control brain sections (from normal cases with no NFTs and SPs), BSB staining was not seen (data not shown). Although BSB was designed and tested *in vitro* for binding to Aβ, we hypothesized it may also bind NFTs, because NFTs are also β-pleated fibrils (18). Indeed, well-characterized amyloid-binding dyes such as Congo red and TF-S stain a variety of forms of amyloid including NFTs. Thus, not unexpectedly, dystrophic neurites and NFTs also stained brightly with BSB (Fig. 1*C*), similar to TF-S staining of serial sections (Fig. 1*D*), which revealed equivalent numbers of NFTs. Because BSB specifically and sensitively stained SPs, NFTs, and dystrophic neurites, it is an appropriate probe for AD pathology but should be able to gain access to SPs more readily because of their extracellular location.

The identification of BSB as a marker for AD pathology prompted us to establish optimal staining conditions for this compound. We determined that, whereas 0.01% BSB was sufficient for specific labeling of plaques (data not shown), greatest sensitivity was obtained by using a saturated 50% EtOH solution of BSB (which contained less than 0.5% BSB). Because *in vitro* studies by using BSB bound to synthetic amyloid demonstrate that maximal emission of excited BSB occurs at 520 nm (Z. P. Zhuang and H.F.K., personal communication), both the FITC and UV filter cubes are appropriate for examination of BSB-stained tissue. However, we found that the broader pass UV filter set yielded a more intense fluorescence signal, consistent with the maximal excitation of BSB at 340 nm, determined *in vitro*. Because the use of the UV filter cube reveals higher autofluorescence in human tissue, we used primarily the FITC filter set for postmortem human tissue and the UV filter set for mouse and cell culture experiments.

To test the usefulness of BSB for labeling Aβ plaques in an animal model of amyloid plaque deposition, we used Tg2576 transgenic mice, which express human APP695 with the K670N, M671L Swedish double mutation (8). By 11–13 months of age, Tg2576 mice show prominent Aβ deposition in the cingulate cortex, entorhinal cortex, dentate gyrus, and CA1 hippocampal subfield (8, 19). As expected, BSB effectively labeled Aβ plaques in postmortem cortical sections from 12-mo-old Tg2576 mice (Fig. 1*E*), with similar sensitivity as TF-S (Fig. 1*F*). No specific staining was seen in postmortem sections from control (non-transgenic) mice (data not shown).

BSB Labels Intracellular Aβ in Living Human Fibroblasts. Although BSB is an effective marker for amyloid in fixed tissue, *in vivo* use of BSB for imaging amyloid deposits requires brain penetration. Because membrane permeability confers the ability to cross the BBB, we sought to develop a cell culture assay to test the cell permeability of potential amyloid probes. To generate high levels of intracellular Aβ aggregates, we treated cultured human skin fibroblasts with synthetic $A\beta_{1-42}$ peptide. After endocytosis of the soluble Aβ, the cells accumulate intracellular aggregates of Aβ, which remain stable over several days in culture (20). These Aβ aggregates have been localized to the endosomes and secondary lysosomes by indirect immunofluorescence (20), but it is unclear whether they assembled into Aβ fibrils with β-pleated sheet structure.

To test whether these Aβ aggregates were indeed amyloid, we stained human fibroblasts grown in the presence of synthetic $A\beta_{1-42}$ with BSB and TF-S. After a 24-h incubation in medium containing up to 50 μg/ml $A\beta_{1-42}$, fibroblasts were trypsinized to remove Aβ bound to the cell surface and replated in Aβ free medium. After a 24-h recovery period, cells were fixed, permeabilized, and stained with either BSB or TF-S. In the absence of Aβ treatment, no specific fluorescence staining was observed (Fig. 2 *A* and *D*). After Aβ treatment, numerous small paranuclear deposits of Aβ were detected by both BSB and TF-S (Fig. 2, arrowheads). Large irregularly shaped deposits of Aβ were also observed and may reflect extracellular amyloid that was resistant to trypsinization (Fig. 2, arrows). To control for specificity, we treated cells with a reverse Aβ peptide ($A\beta_{42-1}$); these cells showed no specific fluorescence staining (data not shown). As BSB and TF-S do not recognize soluble Aβ but bind only aggregated Aβ in the

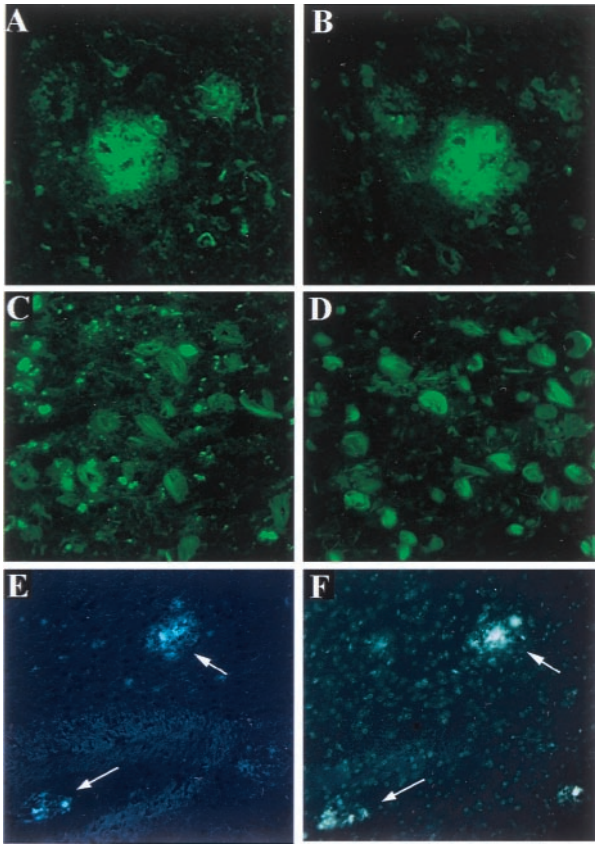

Fig. 1. BSB fluorescently labels AD SPs and NFTs with similar intensity as TF-S. Cortical (*A* and *B*) and hippocampal (*C* and *D*) sections from patients ($n = 3$) with postmortem-confirmed AD were stained with BSB (*A* and *C*) or TF-S (*B* and *D*). Postmortem sections from 12-mo-old Tg2576 mice were similarly stained with BSB (*E*) or TF-S (*F*). Shown are representative SP with accompanying neuritic pathology taken at ×400 (*A* and *B*), abundant NFTs (×400, *C* and *D*), or mouse cortical plaques taken at ×200 (arrows in *E* and *F*).

form of amyloid (Z. P. Zhuang and H.F.K., personal communication) (21), these data demonstrate that intracellular $A\beta_{1-42}$ in these human fibroblasts exists as amyloid.

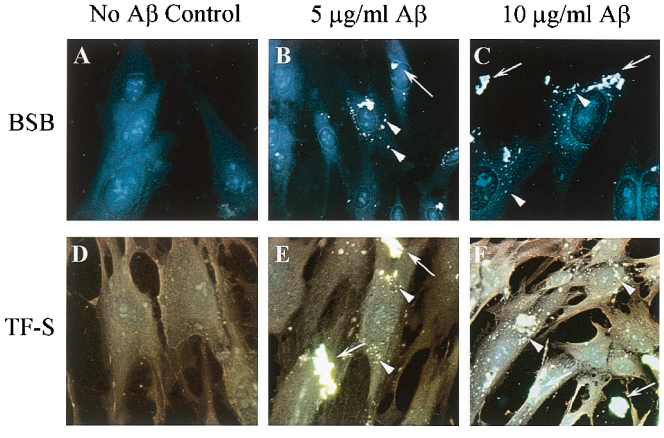

Fig. 2. Aβ-treated human fibroblasts accumulate TF-S-positive/BSB-positive intracellular amyloid. Untreated fibroblasts (*A* and *D*), fibroblasts treated with 5 μg/ml Aβ (*B* and *E*), and fibroblasts treated with 10 μg/ml Aβ (*C* and *F*) were trypsinized, replated on cover slips, fixed, and stained with BSB (*A–C*) or with TF-S (*D–F*). Examples of small paranuclear intracellular amyloid aggregates are labeled with arrowheads. Arrows label examples of extracellular amyloid aggregates. Images shown (×400) are representative of three separate experiments.

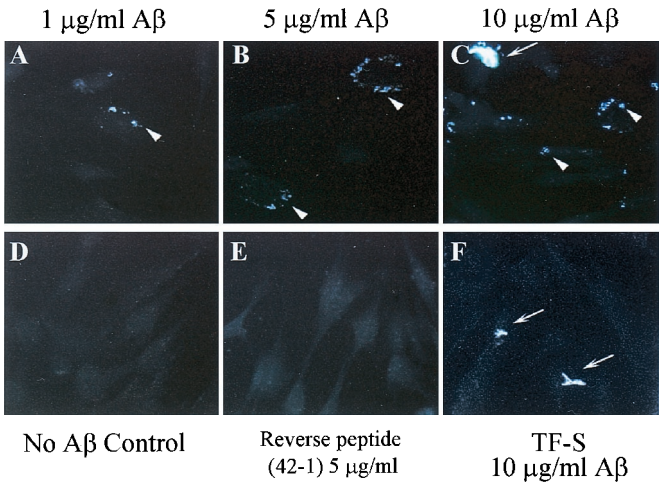

Fig. 3. BSB but not TF-S labels intracellular amyloid aggregates in living cells. Fibroblasts treated with 1 μg/ml Aβ (*A*), 5 μg/ml Aβ (*B*), 10 μg/ml Aβ (*C* and *F*), untreated with Aβ (*D*) or treated with 5 μg/ml of the reverse Aβ sequence peptide $A\beta_{42-1}$ (*E*), were trypsinized, replated, and incubated with for 2 h with the addition of 0.005% BSB (*A–E*) or 0.005% TF-S (*F*) to the culture medium. Cells were fixed and viewed directly under the fluorescence microscope. Intracellular amyloid aggregates were detected with BSB only and are labeled with arrowheads. Extracellular amyloid aggregates were detected with both BSB and TF-S and are labeled with arrows. Images shown (×400) are representative of three separate experiments.

Because fibroblasts treated with $A\beta_{1-42}$ developed intracellular amyloid, we hypothesized that they were a suitable model to test permeability of amyloid-binding compounds. Thus we pretreated fibroblasts with $A\beta_{1-42}$, trypsinized as before and incubated the living cells with medium containing 0.005% BSB or 0.005% TF-S for 2 h. Cells were washed thoroughly, fixed, and examined directly by fluorescent microscopy. Untreated cells (Fig. 3*D*) or cells treated with the Aβ reverse peptide (Fig. 3*E*) showed no intracellular labeling. By contrast, living cells treated with BSB showed intense paranuclear staining of intracellular aggregates of Aβ (Fig. 3 *A–C*, arrowheads). Staining of intracellular Aβ aggregates increased with Aβ concentration, and occasional extracellular Aβ aggregates were detected, especially after treatment with high levels of Aβ (Fig. 3*C*, arrow). To confirm the extracellular location of these large Aβ aggregates, we incubated living cells with TF-S, which is not cell permeable. Incubation of Aβ-treated fibroblasts with TF-S labeled only these large extracellular Aβ aggregates (Fig. 3*F*, arrows) but not the small paranuclear Aβ aggregates seen with BSB. Aβ-treated

Table 1. Quantitation of Aβ recovery from Aβ-treated fibroblasts

Synthetic Aβ added	μg/ml	$A\beta_{1-42}$ recovered, fmol/sample†	BSB-stained Aβ aggregates‡
$A\beta_{1-42}$	0	59 ± 41	None
	1	6,046 ± 1,201	+
	5	17,710 ± 1,743	++
	10	39,410 ± 11,712	+++
	50	66,792 ± 14,264	+++
$A\beta_{42-1}$	5	34 ± 24	None

*Fibroblasts were treated with Aβ, trypsinized, and replated as before.
†Cells were lysed in formic acid, and intracellular $A\beta_{1-42}$ was quantitated by sandwich ELISA. Means and standard deviations for three separate experiments (each performed in duplicate) are shown.
‡Qualitative detection of Aβ aggregates after incubation of living cells with BSB.

NEUROBIOLOGY

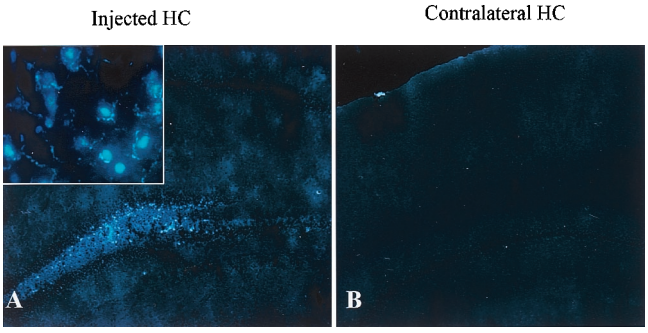

Fig. 4. Intrahippocampal injection of BSB in control mice detects no plaque-like structures. BSB was stereotactically injected into the hippocampus of a 12-mo-old control mouse. Eighteen hours later, frozen sections reveal diffuse hippocampal labeling (*A*) with occasional specific uptake by neurons (*Inset*, ×400) at the site of injection. On the contralateral side, no staining over background is apparent (*B*). Images shown are at ×100 and are representative of three mice.

fibroblasts incubated with vehicle only (i.e., no TF-S or BSB) showed no specific fluorescent labeling (data not shown).

Because this *in vitro* model allowed us to quantify accurately the amount of intracellular aggregated Aβ, we next determined the minimum level of Aβ required for detectable BSB staining. We treated fibroblasts with varying concentrations of Aβ, trypsinized and replated the cells as before, lysed the cells in 70% formic acid, and quantitated intracellular Aβ_{1-40} and Aβ_{1-42} by sandwich ELISA. Levels of Aβ_{1-40} were not significant in any sample. As shown in Table 1, there was a linear relationship between Aβ_{1-42} added to the culture media and Aβ_{1-42} recovered from the cells. Thus, we were able to calibrate the sensitivity of BSB staining and determined that the lowest level of intracellular Aβ resulting in robust staining was approximately 18 pmols Aβ per cover slip ($\approx$0.7 pg/cell distributed in $\approx 1 \times 10^5$ cells).

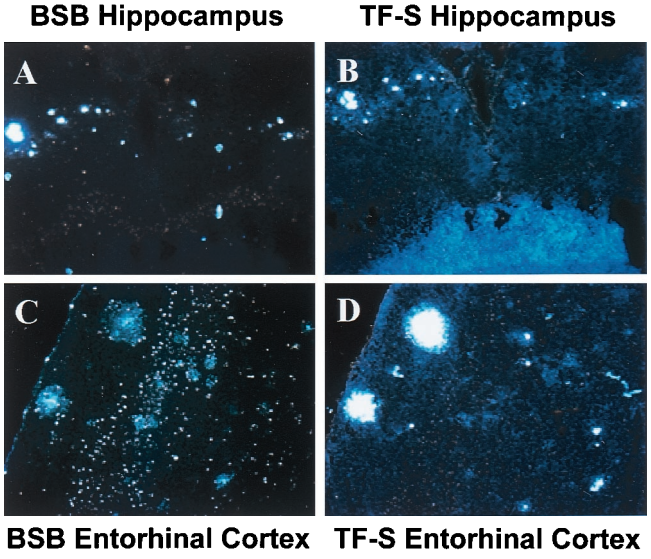

Fig. 5. Intrahippocampal injection of BSB in Tg2576 mice specifically labels abundant plaque pathology in the hippocampus and entorhinal cortex. BSB was stereotactically injected into the hippocampus of a 12-mo-old Tg2576 mouse. Eighteen hours later, frozen sections revealed prominent labeling of SPs in the ipsilateral (*A Left*) and contralateral (*A Right*) hippocampi. SPs are also clearly visible in the entorhinal cortex (*C*). After imaging for BSB staining, sections were stained with TF-S and reimaged (*B* and *D*). Images shown are at ×200 and are representative of two mice.

BSB Stains Aβ Deposits in Living Tg2576 Mice. BSB staining of amyloid in living cells and staining of plaques in fixed Tg2576 brains prompted us to test the usefulness of BSB in living Tg2576 mice. Thus, we stereotactically injected BSB into the hippocampi of anesthetized 12-mo-old Tg2576 and control mice. Mice were killed 18 h after injection, and frozen sections were prepared and examined by fluorescent microscopy. Injection of BSB into hippocampi of control mice resulted in diffuse nonspecific labeling of hippocampal parenchyma (Fig. 4*A*) with sporadic bright staining of granular neurons in the dentate gyrus, suggesting that the neurons are capable of taking up BSB (Fig. 4*A Inset*), but there was no plaque-like staining. Contralateral to the injection site (Fig. 4*B*), there was no discernable staining as compared with injection of vehicle alone. In contrast, injection of BSB into aged Tg2576 mice resulted in rapid labeling of Aβ plaques. These amyloid plaques were clearly stained at 30 min and 3 h after injection with low background staining (data not shown). At 18 h after injection, background BSB staining was nearly completely absent, and plaques remained brightly stained (Fig. 5). BSB-stained plaques were observed bilaterally in the hippocampus, with greater intensity of staining on the ipsilateral side (shown on Fig. 5*A Left*). Less intensely stained plaques were also detected bilaterally in the entorhinal cortex (Fig. 5*C*), suggesting diffusion of BSB from the site of injection. To compare the sensitivity of *in vivo* BSB staining with postmortem TF-S staining, frozen sections were stained with TF-S. As shown in Fig. 5*B*, TF-S staining of hippocampal sections did not increase number or intensity of plaque staining as compared

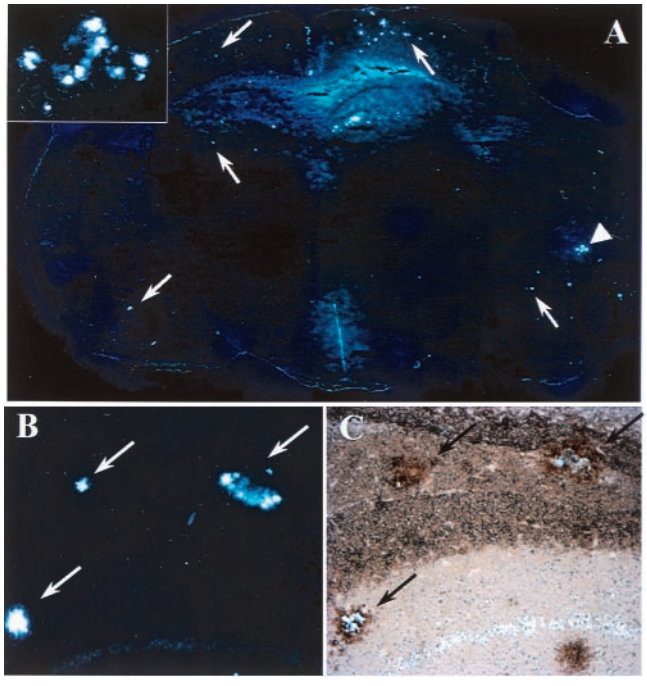

Fig. 6. Injection of BSB into the lateral ventricle of living Tg2576 mice labels abundant plaques throughout the brain. BSB was stereotactically injected into the left lateral ventricle of a 12-mo-old Tg2576 mouse. Eighteen hours later, frozen sections revealed prominent labeling of SPs in the hippocampus, entorhinal cortex, cingulate gyrus, and other affected brain regions ipsilaterally (*Right*) and contralaterally (*Left*). (*A*) A composite of 12 × 20 fields is shown, with examples of SPs marked by arrows. A cluster of entorhinal cortical SPs (marked with an arrowhead) are shown in *Inset* (×400). Representative sections were first imaged for BSB fluorescence (*B*) and then immunostained for Aβ by using the mAb 4G8 (*C*). BSB labeled the majority of plaques detected by immunostaining (arrows). The intensity of BSB labeling allowed simultaneous visualization of fluorescence and 3,3′-diaminobenzidine tetrahydrochloride staining. Images shown are representative of two mice.

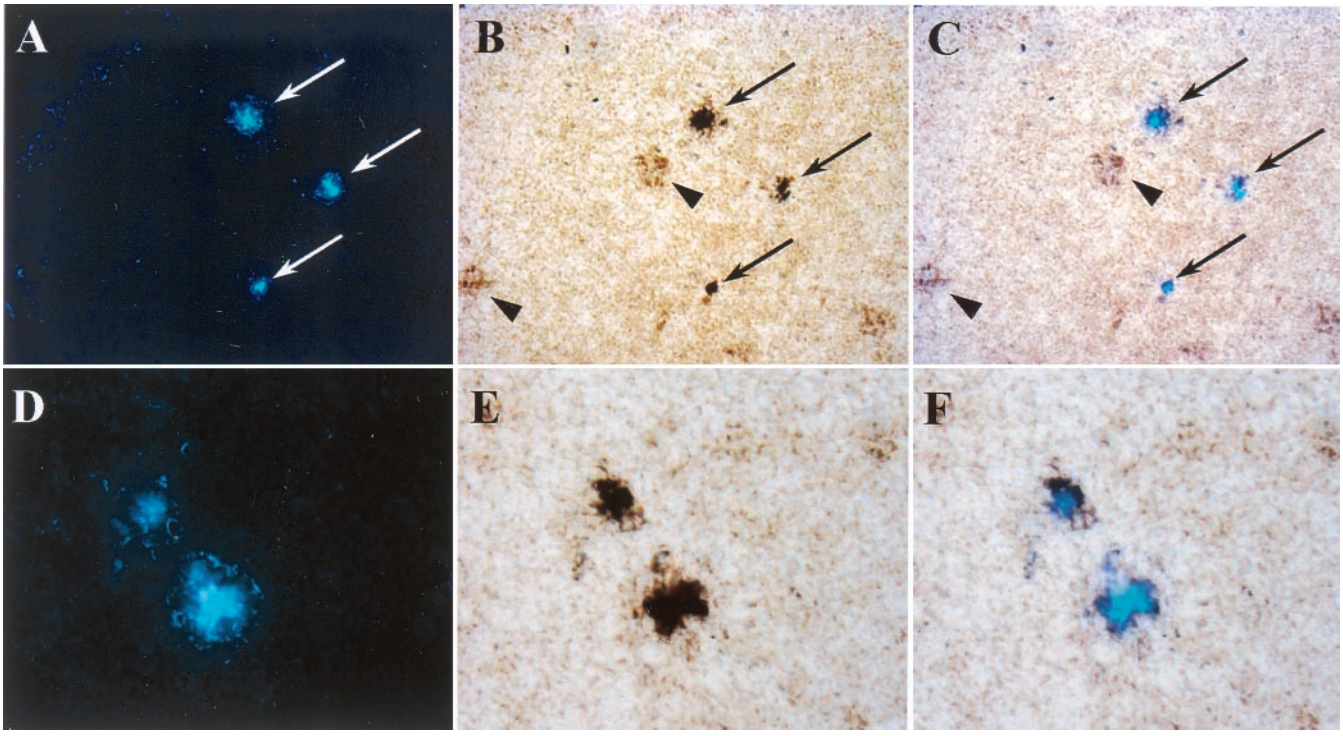

Fig. 7. i.v. injection of BSB results in abundant labeling of SPs in Tg2576 mice. BSB was injected into the tail vein of a 12-mo-old Tg2576 mouse. Eighteen hours later, direct examination of frozen sections of the brain revealed prominent BSB labeling of plaques in the hippocampus (*A*, ×200), entorhinal cortex (*D*, ×400), cingulate gyrus, and other affected brain regions bilaterally. Sections were subsequently immunostained with the Aβ specific antiserum 2332 (*B* and *E*). Fluorescent and light microscopic images were digitally overlain (*C* and *F*), revealing the specificity of BSB plaque labeling (arrows). Arrowheads (*B*) show less intensely Aβ immunopositive plaques that were not labeled with BSB. Images shown are representative of three mice.

with BSB staining. In contrast, intensity of plaque labeling in the entorhinal cortex was enhanced after TF-S staining (Fig. 5*D*). In neither case did TF-S staining reveal plaques that were unlabeled by BSB.

To deliver BSB to a greater volume of brain parenchyma, we injected BSB into the lateral ventricles of 12-mo-old Tg2576 mice. As shown in Fig. 6 (arrows), 18 h after injection into the left lateral ventricle, plaques were labeled bilaterally throughout the hippocampus, cingulate cortex, and entorhinal cortex, demonstrating penetration of BSB throughout multiple brain regions. Both single plaques (Fig. 6*B*) and complex clusters of plaques (Fig. 6*A Inset*) were brightly labeled. To assess the specificity and sensitivity of antemortem BSB plaque labeling, Aβ deposition in postmortem frozen sections was visualized by immunohistochemistry with an Aβ-specific antibody (4G8). BSB staining was discernable during simultaneous visible and fluorescent illumination of sections, allowing direct comparison of BSB labeling (shown alone in Fig. 6*B*) and Aβ immunostaining (Fig. 6*C*). All BSB-labeled deposits (arrows) were positive for Aβ, suggesting that BSB labeling was highly specific. Similarly, nearly all Aβ positive plaques had been labeled by BSB, confirming the high sensitivity of BSB when used *in vivo*. The few Aβ positive plaques that did not stain with BSB may contain mostly nonfibrillar Aβ and are also TF-S negative (data not shown).

To test the permeability of BSB through the BBB, we injected the compound intravenously in Tg2576 mice. We examined brain tissue 18 h later and found BSB-labeled amyloid plaques throughout affected brain regions (Fig. 7 *A* and *D*). Although staining intensity was lower than after intraventricular injection, plaques were still clearly discernible, and background staining was very low. To test the sensitivity and specificity of BSB labeling, we again visualized Aβ deposition by immunostaining (Fig. 7 *B* and *E*). Overlay of fluorescent and light microscopic images revealed absolute specificity of BSB labeling for amyloid plaques (Fig. 7 *C* and *F*). BSB staining consistently labeled the plaques with greatest Aβ immunoreactivity (Fig. 7*C*, arrows) and did not label plaques that were less intensely Aβ-positive (Fig. 7*B*, arrowheads). Lack of BSB staining may result from lower total amounts of Aβ or from lower proportions of fibrillary Aβ in these plaques. Alternatively, it may reflect binding of amounts of BSB below the levels of sensitivity for detection by fluorescent microscopy.

Discussion

BSB is a probe designed to penetrate the BBB and bind brain Aβ deposits with high affinity to enable radiological imaging of SPs in the brains of living patients for monitoring the temporal progression of AD and the clearance of SPs in response to antiamyloid therapies. Indeed, radiological visualization of plaques and tangles may aid in the diagnosis of AD but the usefulness of diagnostic imaging agents *in vivo* depends largely on their sensitivity and specificity for these lesions as well as their ability to penetrate the BBB.

Thus, to evaluate BSB for *in vivo* use as a probe to detect Aβ deposits, we first characterized the ability of BSB to label AD amyloid plaques. We determined optimal conditions for staining SPs in AD brain sections with BSB and showed that BSB specifically labels plaques and tangles with high sensitivity. Although SPs and NFTs are formed by different proteins, they share the β-pleated sheet structure characteristic of amyloid. Thus, like Congo red and TF-S, the specificity of BSB for these two hallmark AD lesions appears to be determined by the structure of the fibrils in these lesions rather than by their protein subunits.

Although BSB is lipophilic *in vitro* (Zhuang *et al.*, personal communication), we sought to test this directly in living cells, and we designed a cell culture assay for membrane permeability by using human fibroblasts that accumulate intracellular aggregated Aβ after exposure to synthetic Aβ (20). Although the presence of intracellular Aβ aggregates has been well documented in a variety of cell culture systems (17, 20, 22–24), we demonstrated that internalized Aβ form intracellular amyloid because BSB (which is specific for β-pleated sheet structure), when added to the culture medium of Aβ-treated living fibroblasts, specifically labeled this pool of internalized Aβ. Our observation that low concentrations of BSB were sufficient to brightly label intracellular amyloid suggests that BSB must be concentrated inside cells containing Aβ amyloid. Indeed, we found that BSB detected as little as 18 pmols Aβ in 1×10^5 cells, whereas >2,000 pmols Aβ per gram of tissue are typically found in AD brains (25).

Further, because BSB injected into the brains of transgenic mouse models of AD amyloidosis labeled plaques *in vivo*, BSB satisfies a crucial test for an amyloid-binding probe. Indeed, to our knowledge this is the first demonstration that an amyloid-specific probe binds to plaques *in vivo*, and we found that BSB labeled plaques with greater specificity (lower background staining) than in the postmortem AD brain, and BSB that was bound to amyloid plaques remained stable for at least 18 h. However, to quantify the stability and binding kinetics of BSB [(125)I]-radiolabeled BSB will need to be developed and tested, and this is now the focus of studies conducted in our laboratory.

Finally, we demonstrated that BSB enters the brain and labels plaques after i.v. injection. Because BSB binds Aβ with high affinity and with high stability *in vivo*, it is possible that the continued brain penetration of only very low levels of BSB is sufficient to result in the accumulation of BSB in plaques over time. Indeed, plaques were labeled more strongly after repeated i.v. injections of BSB over several hours.

Because accumulation of aggregated fibrils with a β-pleated structure is a common neuropathological feature of several neurodegenerative diseases, an amyloid-binding probe such as BSB should detect pathology in diseases other than AD. Indeed, BSB binds to NFTs (Fig. 1*C*) and Lewy bodies, as well as glial cell inclusions (data not shown) in brains sections from AD, Parkinson's disease, and multiple-system atrophy patients, respectively. Thus, it remains to be determined whether such a probe will have the highest affinity for amyloid, and whether it is able to detect the anatomical distribution of SP with sufficient precision to allow differential diagnosis of these diseases.

In summary, BSB has several properties that suggest that BSB or a BSB-like derivative may become a useful probe for imaging AD pathology *in vivo*: (*i*) BSB labels Aβ amyloid plaques specifically and sensitively; (*ii*) BSB is cell permeable; (*iii*) BSB distributes throughout the brain after a single intracerebral injection; (*iv*) after binding to plaques, BSB is stable *in vivo*; and (*v*) BSB crosses the BBB of transgenic mouse models of AD amyloidosis and labels Aβ deposits. Although future studies are required to test the toxicity, stability, and biodistribution of BSB, our data suggest that BSB can serve as a useful prototype ligand for developing probes to establish a diagnosis of AD in living patients.

We gratefully thank Dr. K. Hsiao for providing the Tg2576 mice. We also thank Dr. N. Suzuki and Takeda Pharmaceutical, Inc., for providing the mAbs for the Aβ sandwich ELISA. This work was supported by grants from the National Institute on Aging and by the estate of Mona Schneidman. D.M.S. is the recipient of a Medical Scientist Training Program Predoctoral Fellowship from the National Institutes of Health.

1. Selkoe, D. J. (1999) *Nature (London)* **399,** A23–A31.
2. Cai, X. D., Golde, T. E. & Younkin, S. G. (1993) *Science* **259,** 514–516.
3. Suzuki, N., Cheung, T. T., Cai, X. D., Odaka, A., Otvos, L. J., Eckman, C., Golde, T. E. & Younkin, S. G. (1994) *Science* **264,** 1336–1340.
4. Borchelt, D. R., Thinakaran, G., Eckman, C. B., Lee, M. K., Davenport, F., Ratovitsky, T., Prada, C. M., Kim, G., Seekins, S., Yager, D., *et al.* (1996) *Neuron* **17,** 1005–1013.
5. Duff, K., Eckman, C., Zehr, C., Yu, X., Prada, C. M., Perez-tur, J., Hutton, M., Buee, L., Harigaya, Y., Yager, D., *et al.* (1996) *Nature (London)* **383,** 710–713.
6. Scheuner, D., Eckman, C., Jensen, M., Song, X., Citron, M., Suzuki, N., Bird, T. D., Hardy, J., Hutton, M., Kukull, W., *et al.* (1996) *Nat. Med.* **2,** 864–870.
7. Games, D., Adams, D., Alessandrini, R., Barbour, R., Berthelette, P., Blackwell, C., Carr, T., Clemens, J., Donaldson, T. & Gillespie, F. (1995) *Nature (London)* **373,** 523–527.
8. Hsiao, K., Chapman, P., Nilsen, S., Eckman, C., Harigaya, Y., Younkin, S., Yang, F. & Cole, G. (1996) *Science* **274,** 99–102.
9. Holcomb, L., Gordon, M. N., McGowan, E., Yu, X., Benkovic, S., Jantzen, P., Wright, K., Saad, I., Mueller, R., Morgan, D., *et al.* (1998) *Nat. Med.* **4,** 97–100.
10. Schenk, D., Barbour, R., Dunn, W., Gordon, G., Grajeda, H., Guido, T., Hu, K., Huang, J., Johnson-Wood, K., Khan, K., *et al.* (1999) *Nature (London)* **400,** 173–177.
11. Vassar, R., Bennett, B. D., Babu-Khan, S., Kahn, S., Mendiaz, E. A., Denis, P., Teplow, D. B., Ross, S., Amarante, P., Loeloff, R., *et al.* (1999) *Science* **286,** 735–741.
12. Klunk, W. E., Debnath, M. L. & Pettegrew, J. W. (1994) *Neurobiol. Aging* **15,** 691–698.
13. Klunk, W. E., Debnath, M. L. & Pettegrew, J. W. (1995) *Neurobiol. Aging* **16,** 541–548.
14. Dezutter, N. A., Dom, R. J., de Groot, T. J., Bormans, G. M. & Verbruggen, A. M. (1999) *Eur. J. Nucleic Med.* **26,** 1392–1399.
15. Klunk, W. E., Hamilton, R. L., Styren, S. D., Styren, G., Debnath, M. L., Mathis, C. A., Mahmood, A. & Hsiao, K. K. (1997) *Soc. Neurosci. Abstr.* **23,** 1638.
16. The Ronald and Nancy Reagan Research Institute of the Alzheimer's Association and the NIA Working Group (1998) *Neurobiol. Aging* **19,** 109–116.
17. Skovronsky, D. M., Doms, R. W. & Lee, V. M.-Y. (1998) *J. Cell Biol.* **141,** 1031–1039.
18. Kirschner, D. A., Abraham, C. & Selkoe, D. J. (1986) *Proc. Natl. Acad. Sci. USA* **83,** 503–507.
19. Irizarry, M. C., Soriano, F., McNamara, M., Page, K. J., Schenk, D., Games, D. & Hyman, B. T. (1997) *J. Neurosci.* **17,** 7053–7059.
20. Knauer, M. F., Soreghan, B., Burdick, D., Kosmoski, J. & Glabe, C. G. (1992) *Proc. Natl. Acad. Sci. USA* **89,** 7437–7441.
21. LeVine, H. (1993) *Protein Sci.* **2,** 404–410.
22. Yang, A. J., Knauer, M., Burdick, D. A. & Glabe, C. (1995) *J. Biol. Chem.* **270,** 14786–14792.
23. Burdick, D., Kosmoski, J., Knauer, M. F. & Glabe, C. G. (1997) *Brain Res.* **746,** 275–284.
24. Morishima-Kawashima, M. & Ihara, Y. (1998) *Biochemistry* **37,** 15247–15253.
25. Wang, J., Dickson, D. W., Trojanowski, J. Q. & Lee, V. M.-Y. (1999) *Exp. Neurol.* **158,** 328–337.